

Axial HoloTile: Extended Depth-of-Focus of Dynamic Holographic Light Projections

Andreas Erik Gejl Madsen, Jesper Glückstad

SDU Centre for Photonics Engineering, University of Southern Denmark,
Campusvej 55, 5230 Odense-M

E-mail: gejl@mci.sdu.dk, jegl@sdu.dk

Abstract. This publication extends the HoloTile framework to three dimensions, introducing the ability to generate arbitrary dynamic patterns composed of extended depth-of-field non-diffractive beamlets with theoretically 100% diffraction efficiency. In particular, we demonstrate experimentally the generation of speckle-reduced reconstruction patterns, consisting of spatially multiplexed extended Bessel-like beamlets, implemented on a phase-only spatial light modulator (SLM).

Due to the inherent separation of the tiled subhologram and the point spread function shaping hologram in HoloTile, we show that the reconstruction amplitude can be expressed as a simple convolution of the contributions from the two holograms. This results in a discretely sampled reconstruction, with each spatial frequency component exhibiting long DoF with characteristic Bessel beam properties. This separation facilitates spatial and temporal multiplexing of both contributions, and allows for real-time dynamic patterning with extended DoF. Additionally, a geometric analysis is included, allowing for the direct calculation of the propagation characteristics of the beamlets.

Keywords: HoloTile, Holography, Propagation, 3D-printing, Volumetric Additive Manufacturing

1. Background

Dynamic manipulation of light in two and three dimensions is crucial for modern scientific research and practical applications, enhancing control over light-matter interactions. This capability drives advancements in neuroscience [1, 2], microbiology, optical manipulation [3–5], materials processing [6], microfabrication [7, 8], and more.

This study extends the HoloTile [9–13] framework by introducing extended depth-of-focus (DoF) beamshaping for increased axial control, enabling real-time dynamic light shaping of long-propagating beamlets. This advancement supports applications in volumetric additive manufacturing (VAM) [14–19], laser material processing (LMP) [20–22], laser-based lithography [23], and optical coherence tomography (OCT) [24, 25]. In particular, non-diffractive beams with extended depth-of-focus (DoF) such as pin beams [26, 27], needle beams [28], and Bessel beams [29], etc. are of significant interest in numerous areas due to their attractive properties for e.g., self-healing beamlets and parallel optical particle guidance along the optical axis [30, 31]. In this publication, one instance of such beams are shown to be incorporated into the HoloTile framework; the Bessel beam.

Considering carefully the creation of HoloTile holograms; the combination of a tiled object hologram H_{sub} and a separate PSF hologram H_{PSF} , allows for several interesting conclusions to be drawn. The hologram plane, as it is displayed on the phase only spatial light modulator (SLM) can be expressed as

$$H_{\text{SLM}}(\xi, \eta; t) = H_{\text{PSF}} \cdot \sum_{i,j=0}^{N_t} \delta(\xi - i\ell_s, \eta - j\ell_s) \otimes H_{\text{sub}} \quad (1)$$

where ℓ_s is the physical size of the subholograms and \otimes denotes the colvolution operation. The tiling is expressed by the convolution of a comb array and the subhologram. From this, the field in the focal plane can be expressed directly by the optical Fourier transform of a convex lens or by free-space Fraunhofer propagation:

$$\begin{aligned} A_f(x, y; t) &\propto A_{\text{PSF}} \otimes \sum_{\substack{m,n \\ =-\infty \\ =\infty}}^{\infty} \delta\left(x - \frac{m}{\ell_s}, y - \frac{n}{\ell_s}\right) \mathcal{F}\{H_{\text{sub}}\} \\ &\propto A_{\text{PSF}}(x, y, z; t) \otimes A_{\text{sub}}\left(x - \frac{m}{\ell_s}, y - \frac{n}{\ell_s}; t\right) \end{aligned} \quad (2)$$

where A_{PSF} is the Fourier transform of the PSF shaping hologram, and A_{sub} is the Fourier transform of the subhologram which, due to the tiling operation, is only sampled and thus defined in specific locations defined by the spatial frequency comb array $\sum_{m,n=-\infty}^{\infty} \delta\left(x - \frac{m}{\ell_s}, y - \frac{n}{\ell_s}\right)$.

The aperture of the SLM, the input beamshape and, in turn, the inherent optical point spread function (PSF), are included in H_{PSF} and A_{PSF} , respectively. Thus, $|A_{\text{sub}}|^2$ defines an intensity pattern of regularly spaced points, which may be modulated freely, akin to enabling or disabling single pixels on a digital display. The PSF reconstruction A_{PSF} , however, governs the shape of each of the points in A_{sub} . Both the shape and location[‡] of the PSF can be modulated independently from A_{sub} . This simple separation of terms contributing to the final reconstruction allows for greatly increased illumination and aberration control. Importantly for this publication, the shape of the PSF naturally also extends axially. This effectively means that any beam shape, axially extended or otherwise, can be multiplexed spatially and temporally in any given diffractive pattern, hence the dependence on z and t in A_{PSF} and t in A_{sub} . In the following sections, we demonstrate the generation of extended DoF Bessel beams, and their incorporation into the HoloTile framework.

2. HoloTile Bessel Beam Generation

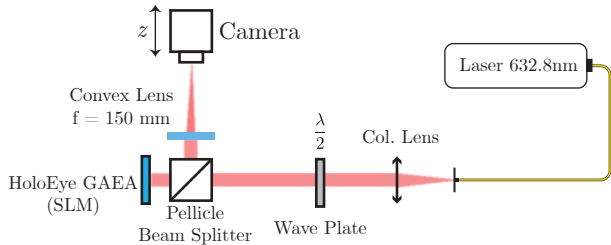
The ring beam shaper defined in the HoloTile framework is given by the phase profile

$$\phi_{\text{ring}}(r) = -\beta r \quad (3)$$

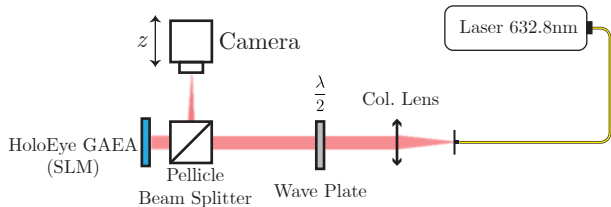
where r is the radius from the optical axis in the hologram plane, $\beta = \frac{2\pi r_0}{f\lambda}$, r_0 is the radius of the desired ring, f is the focal length of the Fourier transforming lens, and λ denotes wavelength. In the focal plane of the Fourier transform lens, the reconstruction shows, as expected, the shape defined by the subhologram H_{sub} in which each point in the spatial frequency grid is shaped into well-defined rings.

Interestingly, as the observation plane is moved axially along the propagation axis a specific distance from the Fourier plane, each ring converges to a point and continues to propagate as a Bessel-like beamlet

[‡] Within the unit cell of each reconstruction point.



(a) Lensed optical system. The SLM modulated field is optically Fourier transformed by a physical convex lens.



(b) Lensless optical system. The SLM modulated field is optically Fourier transformed by a convex lens phase superimposed on the SLM.

Figure 1: The experimental setups for capturing lensed and lensless holographic reconstructions. A fiber coupled HeNe laser is collimated and incident on a phase-only SLM. The modulated reflected light is diverted in a beam splitter and captured directly in camera.

[32]. As the propagation continues, the lobes of the Bessel beamlets expand to be larger than the original ring, at which point spatial intra-spectral interference can occur. A simplified illustration of the Bessel beam generation is shown in Figure 2. Importantly, since the PSF shaping hologram directs all light into the sampled spatial frequency components, the reconstructions have a theoretical diffraction efficiency of 100%.

With the separation of pattern and output pixel shape expressed in Equation (2), each point in the output pattern A_{sub} is shaped, and will propagate, with Bessel beam characteristics.

2.1. Geometric Characterization

As previously remarked, there exists a characteristic distance between the focal plane in which the rings are clearly defined, and what might be considered the beginning of the Bessel beam propagation. Furthermore, there is also a limit to the propagation length over which the lateral extent of the Bessel beams can be considered smaller than the unit cell of HoloTile, i.e., the diameter of the Bessel generating rings. These characteristics can be approximated, following a 2D geometric analysis of the system in Figure 2. Let the focal length of a convex lens be f , and place a negative

axicon phase in accordance with Equation (3) in the front focal plane of the lens. In the back focal plane, the characteristic ring pattern forms following the rotationally symmetric focus of the tilt of the axicon. Following the back focal plane, the ring defocuses, until the two rays originating from the outer radii of the axicon and lens intersect. From this point, Bessel beam interference emerges (red-yellow shaded area), as it would for an annular aperture. In the geometry, it is also apparent that when the innermost rays intersect the outer from the opposite side, light escapes the extent of the propagating Bessel beam (gray shaded area), thus giving rise to interference between adjacent propagating Bessel beams.

The beginning of the Bessel beam is thus given as the z -coordinate at the intersection between the outermost rays. To express the Bessel beam beginning and its effective propagation length, we can approximate the system using the ABCD matrix approach. The final height and angle of the rays in the system is given by

$$\begin{bmatrix} r_f \\ \theta_f \end{bmatrix} = \begin{bmatrix} 1 & d \\ 0 & 1 \end{bmatrix} \begin{bmatrix} 1 & f \\ 0 & 1 \end{bmatrix} \begin{bmatrix} 1 & 0 \\ -1/f & 1 \end{bmatrix} \begin{bmatrix} 1 & f \\ 0 & 1 \end{bmatrix} \begin{bmatrix} r_{\text{SLM}} \\ \theta_0 \end{bmatrix} \quad (4)$$

where r_{SLM} is the characteristic radius of the SLM, d is the free-space propagation following the focal plane, and θ_0 is the deflection angle of the light due to the axicon phase;

$$\begin{aligned} \theta_0 &= \arctan\left(\frac{\lambda\beta}{2\pi}\right) \\ &= \arctan\left(\frac{r_0}{f}\right) \end{aligned} \quad (5)$$

The resulting rays of this geometric model are overlaid on a wave-based propagation simulation in Figure 3. Simplifying Equation (4) yields the final expressions for the outermost ray height and angle :

$$r_f = f\theta_0 - \frac{dr_{\text{SLM}}}{f} \quad (6)$$

$$\theta_f = -\frac{r_{\text{SLM}}}{f} \quad (7)$$

Now, to find the beginning of the Bessel beam, d is isolated in $r_f(r_{\text{SLM}}, \theta_0) = 0$, and can be expressed as

$$B_b = d = \frac{f^2\theta_0}{r_{\text{SLM}}} \quad (8)$$

Similarly, the point at which the lateral extent of the Bessel beam exceeds the generating ring is found by expressing $r_f(r_{\text{SLM}}, \theta_0) = r_f(0, -\theta_0)$ and isolating d :

$$B_e = d = \frac{2f^2\theta_0}{r_{\text{SLM}}} \quad (9)$$

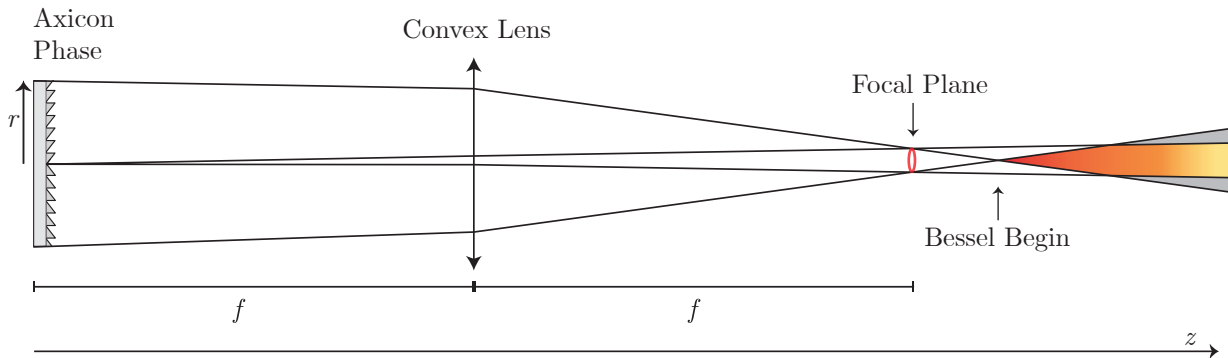


Figure 2: Illustration of the working principle of the ring-generated Bessel beams. A negative axicon phase diverts the incoming light, and is focused to a ring in the focal plane. Following a small propagation, the intersection of the rays from opposite sides of the axicon ring results in the generation of a Bessel beam (orange area). At a certain point, the side-lobes of the Bessel beam extend beyond the extent of the generating ring (gray area).

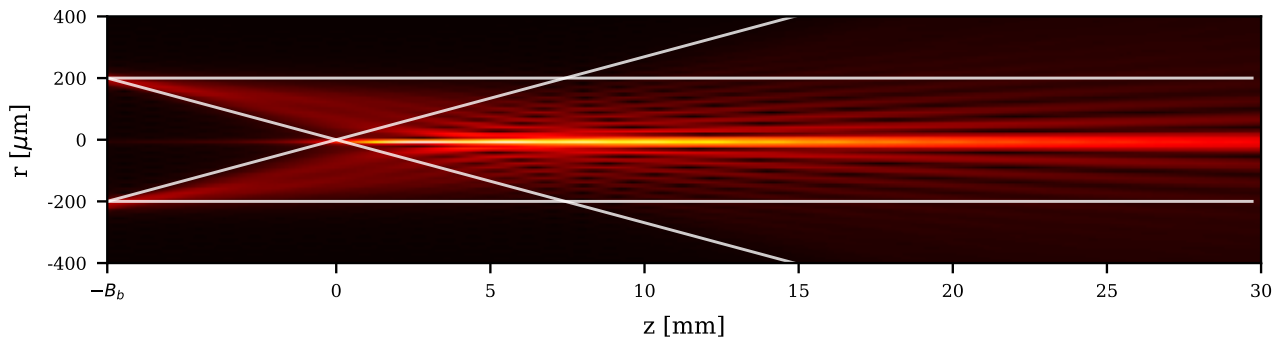


Figure 3: Field amplitude at increasing propagation distances from the beginning of the Bessel beam at $z = 0$ mm to $z = 30$ mm of single ring-generated Bessel beam. Overlaid is the rays resulting from the geometric analysis in Section 2.1. The Bessel-generating ring is located at $z = -B_b$; the characteristic distance between the ring and the beginning of the Bessel beam.

Which results in a propagation length of:

$$B_\ell = B_e - B_b = \frac{f^2 \theta_0}{r_{\text{SLM}}} = \frac{f^2}{r_{\text{SLM}}} \arctan\left(\frac{r_0}{f}\right) \quad (10)$$

Hence, there exists a non-linear relationship between the radius of the Bessel-generating rings r_0 and the propagation length B_ℓ . Although the side lobes of the Bessel beam extend beyond the ring diameter after this point, they are still dim compared to the central lobe. Therefore, the practical propagation length until significant spatial intra-spectral interference is observed is significantly larger, as is observed in Figures 3 to 5. This result can be tied back to the original HoloTile equations [9] in order to express the required number of tiles on the SLM, and thus the required sub-hologram resolution m_{sub} , for a given propagation distance B_ℓ , without the Bessel-generating rings interfering with neighbouring rings.

For the rings to not extend beyond the unit cell of each spatial frequency component, the following inequality can be expressed [9]:

$$r_0 \leq \frac{N_t \lambda f}{4r_{\text{SLM}}} \quad (11)$$

Where N_t is the number of tiles on a square SLM. This requires that

$$N_t \geq \frac{4r_{\text{SLM}}}{\lambda} \tan\left(\frac{B_\ell r_{\text{SLM}}}{f^2}\right) \quad (12)$$

$$\Downarrow \\ m_{\text{sub}} \leq \frac{2r_{\text{SLM}}}{N_t \ell_p} \quad (13)$$

Effectively tying the HoloTile subhologram tiling with the propagation of non-diffractive Bessel beamlets.

3. Experimental Results

To validate the propagation of the axicon-generated Bessel beams, a simple Fourier holography setup is

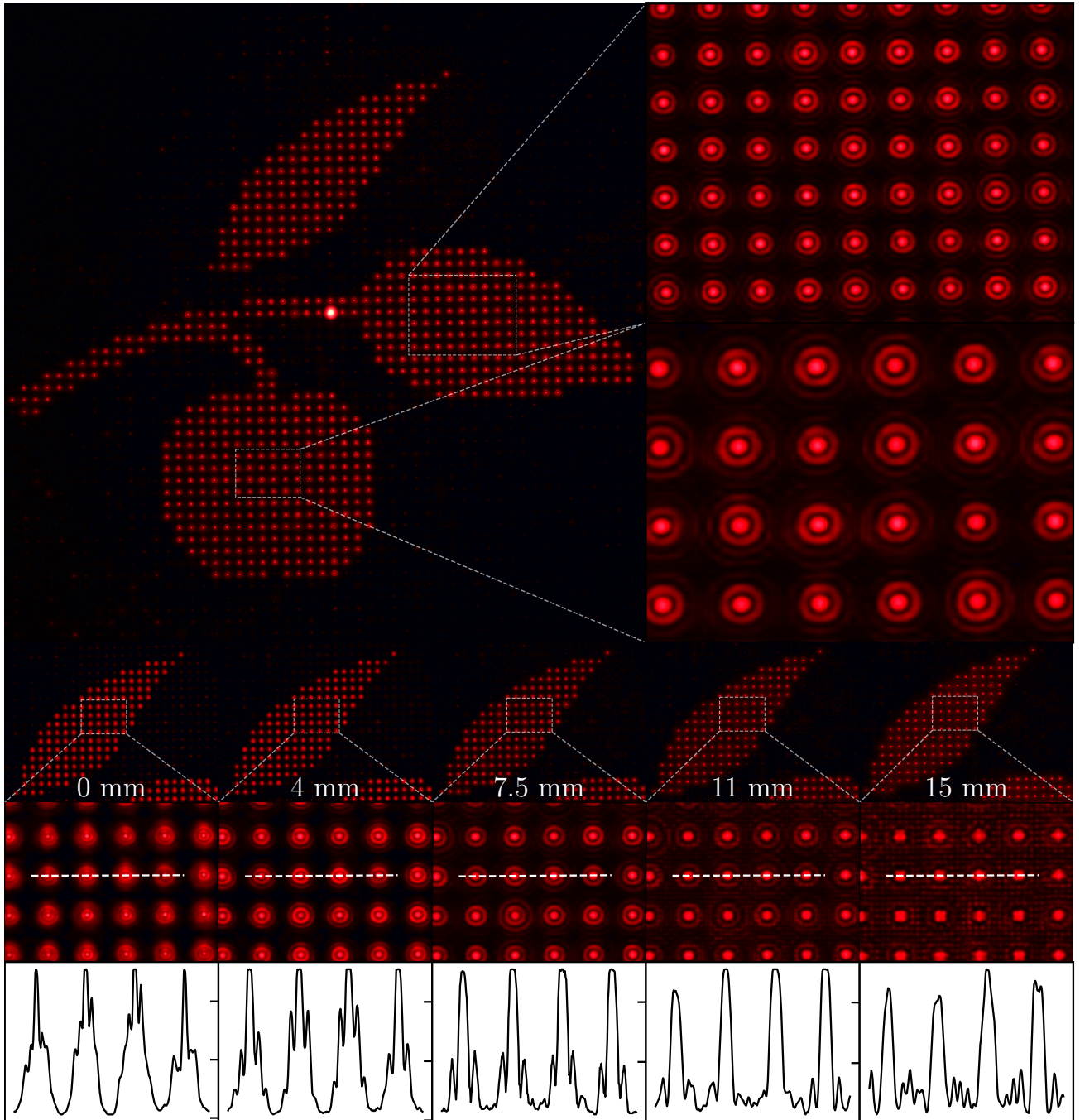


Figure 4

employed, as illustrated in Figure 1a. A fiber-coupled 632nm HeNe laser is collimated and modulated by a HoloEye GAEA phase-only Spatial Light Modulator [33], after which the resultant spatially Fourier transformed patterns are captured by a camera sensor (Canon M6 Mark II) that can be translated axially by an electronic stage. A subhologram corresponding to tile number $N_t = 20$ [9] of the University of Southern Denmark tree branch logo is calculated by

an adaptive weighted Gerchberg-Saxton algorithm [34], and is then tiled to form a 2160×2160 hologram. Then, the separate 2160×2160 PSF shaping hologram is calculated using Equation (3), with $r_{\text{SLM}} = 117.5 \mu\text{m}$ [9]. While the hologram is displayed on the SLM, the camera is alternately capturing photos and moving along the optical axis.

In Figure 4, a summary of the results of the experiment is shown. From the top, the large capture

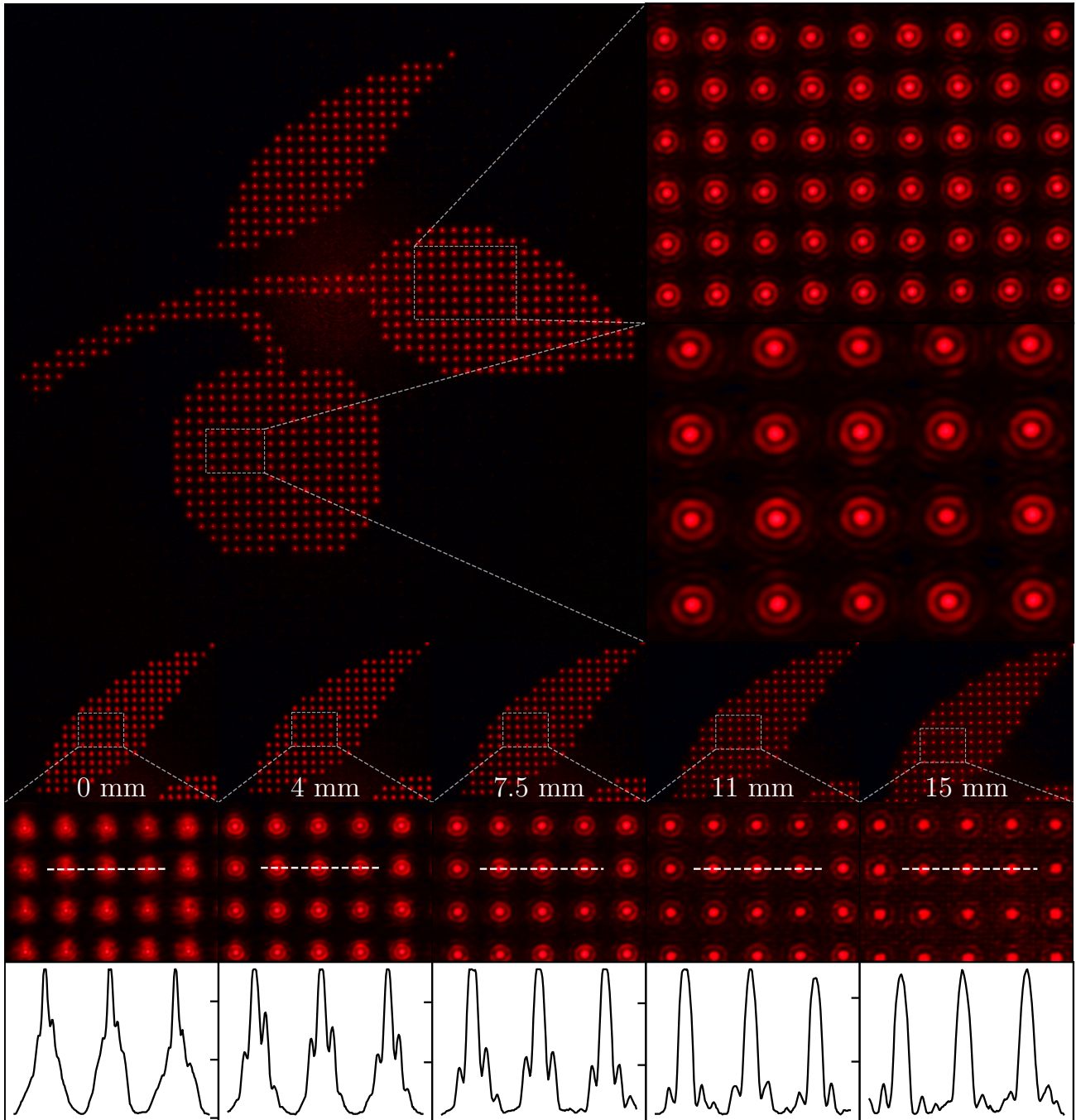


Figure 5

and its insets demonstrate the grid effect associated with HoloTile. Each individual spatial frequency component has been shaped by the PSF shaping hologram. As expected, each component shows the distinct radial oscillations of a Bessel beam. Below, the propagation of the generated Bessel beams is shown. Captures from five different planes spanning 15 mm, along with insets and line profiles through the Bessel beams, demonstrate the extended propagation of the

beams. Additionally, at propagation distances $z = 11.5$ mm and $z = 15$ mm, the beginning of the spatial intra-spectral interference can be observed. However, as was previously noted, the central lobe remains bright compared to the interference.

It is evident in these reconstructions that the Bessel beam PSF shaping allows for extended propagation of the desired pattern. Over the whole propagation distance, the individual output pixels are

well defined, and the variation in brightness is minimal.

HoloTile functions in a lensless configuration as well, by superimposing the phase profile of an equivalent Fourier transforming lens on the SLM. As such, the optical setup in Figure 1a is altered by removing the second lens, and moving the camera and stage to the appropriate focus of $f_{\text{slm}} = 150\text{mm}$. The capture procedure is then repeated, and the results are shown in Figure 5. Again, the Bessel beam shaped reconstructions show good likeness to the pattern throughout the propagation distance, with minimal spatial intra-spectral interference.

It is important to note the enhanced performance achieved by integrating extended Bessel beams with the HoloTile framework, as opposed to simply superimposing a Bessel beam generating phase on a conventional computer-generated hologram (CGH). In a conventional CGH without tiling, the individual spatial frequency components are indistinguishable from one another. Since any beam with extended axial propagation inherently possesses lateral extent, the overlapping and interference of individual point spread functions (PSFs) create inhomogeneities both axially and laterally. By separating the spatial frequency components to a freely chosen degree, the HoloTile framework enables clear and uninterrupted propagation of these beams.

4. Conclusion

The HoloTile framework achieves extended axial control through the generation of extended DoF Bessel beams, independent of target hologram calculations. This independence enables the real-time axial extension of arbitrary patterns using a spatial light modulator.

The extended Bessel beams have been characterized both geometrically and through simulations. Experimental validations in both lensed and lensless configurations demonstrate extended propagation of arbitrary patterns, remaining in focus over a distance of $z = 15\text{ mm}$. The inclusion of Bessel beams is simply one instantiation of extended DoF HoloTile, and future versions may show various other modalities, e.g., pin beams, needle beams, etc. This advancement opens new possibilities for precise and efficient light shaping in various scientific and industrial applications.

Acknowledgments

This work has been supported by the Novo Nordisk Foundation, Denmark (Grand Challenge Program; NNF16OC0021948) and the Innovation Fund Denmark.

References

- [1] E. Papagiakoumou, F. Anselmi, A. Bègue, V. de Sars, J. Glückstad, E. Y. Isacoff, and V. Emiliani, “Scanless two-photon excitation of channelrhodopsin-2,” *Nature Methods*, vol. 7, pp. 848–854, Oct. 2010.
- [2] E. Papagiakoumou, “Optical developments for optogenetics: Optical developments for optogenetics,” *Biology of the Cell*, July 2013.
- [3] D. G. Grier, “A revolution in optical manipulation,” *Nature*, vol. 424, pp. 810–816, Aug. 2003.
- [4] P. J. Rodrigo, V. R. Daria, and J. Glückstad, “Real-time three-dimensional optical micromanipulation of multiple particles and living cells,” *Optics Letters*, vol. 29, p. 2270, Oct. 2004.
- [5] P. Rodrigo, L. Gammelgaard, P. Bøggild, I. Perch-Nielsen, and J. Glückstad, “Actuation of microfabricated tools using multiple GPC-based counterpropagating-beam traps,” *Opt. Express.*, vol. 13, pp. 6899–904, 2005.
- [6] F. Olsen, K. Hansen, and J. Nielsen, “Multibeam fiber laser cutting,” *J. Laser Appl.*, vol. 21, pp. 133–138, 2009.
- [7] S. Kawata, H. Sun, T. Tanaka, and K. Takada, “Finer features for functional microdevices,” *Nature*, vol. 412, pp. 697–8, 2001.
- [8] P. Galajda and P. Ormos, “Complex micromachines produced and driven by light,” *Appl. Phys. Lett.*, vol. 78, p. 249, 2001.
- [9] A. G. Madsen and J. Glückstad, “HoloTile: Rapid and speckle-suppressed digital holography by matched sub-hologram tiling and point spread function shaping,” *Optics Communications*, vol. 525, p. 128876, Dec. 2022.
- [10] A. G. Madsen and J. Glückstad, “Digital holographic-volumetric bio-printing using binary-phase HoloTile on a DMD,” in *Photonics West*, (San Francisco, United States), SPIE, Mar. 2024.
- [11] J. Glückstad and A. E. Gejl Madsen, “HoloTile light engine: New digital holographic modalities and applications,” *Reports on Progress in Physics*, vol. 87, p. 034401, Mar. 2024.
- [12] J. Glückstad, “HOLOGRAPHIC SYSTEM WITH IMPROVED PROJECTION QUALITY (EP 22169752.7),” Apr. 2022.
- [13] J. Glückstad, “HOLOGRAPHIC VOLUMETRIC ADDITIVE MANUFACTURING, EP. 23205831.3,” 2023.
- [14] B. E. Kelly, I. Bhattacharya, H. Heidari, M. Shusteff, C. M. Spadaccini, and H. K. Taylor, “Volumetric additive manufacturing via tomographic reconstruction,” *Science*, vol. 363, pp. 1075–1079, Mar. 2019.
- [15] D. Loterie, P. Delrot, and C. Moser, “High-resolution tomographic volumetric additive manufacturing,” *Nature Communications*, vol. 11, p. 852, Feb. 2020.
- [16] M. Regehly, Y. Garmshausen, M. Reuter, N. F. König, E. Israel, D. P. Kelly, C.-Y. Chou, K. Koch, B. Asfari, and S. Hecht, “Xolography for linear volumetric 3D printing,” *Nature*, vol. 588, pp. 620–624, Dec. 2020.
- [17] M. Shusteff, A. E. M. Browar, B. E. Kelly, J. Henriksson, T. H. Weisgraber, R. M. Panas, N. X. Fang, and C. M. Spadaccini, “One-step volumetric additive manufacturing of complex polymer structures,” *Science Advances*, vol. 3, p. eaao5496, Dec. 2017.
- [18] J. Madrid-Wolff, A. Boniface, D. Loterie, P. Delrot, and C. Moser, “Controlling Light in Scattering Materials for Volumetric Additive Manufacturing,” *Advanced Science*, vol. 9, p. 2105144, Aug. 2022.
- [19] M. I. Álvarez-Castaño, A. G. Madsen, J. Madrid-Wolff, A. Boniface, J. Glückstad, and C. Moser, “Holographic Volumetric Additive Manufacturing,” *arXiv*, 2024.
- [20] P. S. Salter and M. J. Booth, “Adaptive optics in laser processing,” *Light: Science & Applications*, vol. 8, p. 110, Nov. 2019.

- [21] D. Liu, Y. Wang, Z. Zhai, Z. Fang, Q. Tao, W. Perrie, S. P. Edwarson, and G. Dearden, "Dynamic laser beam shaping for material processing using hybrid holograms," *Optics & Laser Technology*, vol. 102, pp. 68–73, June 2018.
- [22] G. Kontenis, D. Gailevičius, N. Jiménez, and K. Staliunas, "Optical Drills by Dynamic High-Order Bessel Beam Mixing," *Physical Review Applied*, vol. 17, p. 034059, Mar. 2022.
- [23] S. Wang, Z. Zhou, B. Li, C. Wang, and Q. Liu, "Progresses on new generation laser direct writing technique," *Materials Today Nano*, vol. 16, p. 100142, Dec. 2021.
- [24] K.-S. Lee and J. P. Rolland, "Bessel beam spectral-domain high-resolution optical coherence tomography with micro-optic axicon providing extended focusing range," *Optics Letters*, vol. 33, p. 1696, Aug. 2008.
- [25] A. Curatolo, P. R. T. Munro, D. Lorenser, P. Sreekumar, C. C. Singe, B. F. Kennedy, and D. D. Sampson, "Quantifying the influence of Bessel beams on image quality in optical coherence tomography," *Scientific Reports*, vol. 6, p. 23483, Mar. 2016.
- [26] Z. Zhang, X. Liang, M. Goutsoulas, D. Li, X. Yang, S. Yin, J. Xu, D. N. Christodoulides, N. K. Efremidis, and Z. Chen, "Robust propagation of pin-like optical beam through atmospheric turbulence," *APL Photonics*, vol. 4, p. 076103, July 2019.
- [27] A. Yu and G. Wu, "Self-healing properties of optical pin beams," *Journal of the Optical Society of America A*, vol. 40, p. 2078, Nov. 2023.
- [28] R. Grunwald and M. Bock, "Needle beams: A review," *Advances in Physics: X*, vol. 5, p. 1736950, Jan. 2020.
- [29] S. N. Khonina, N. L. Kazanskiy, S. V. Karpeev, and M. A. Butt, "Bessel Beam: Significance and Applications—A Progressive Review," *Micromachines*, vol. 11, p. 997, Nov. 2020.
- [30] C. A. Alonzo, P. J. Rodrigo, and J. Glückstad, "Helico-conical optical beams: A product of helical and conical phase fronts," *Optics Express*, vol. 13, p. 1749, Mar. 2005.
- [31] V. R. Daria, D. Z. Palima, and J. Glückstad, "Optical twists in phase and amplitude," *Optics Express*, vol. 19, p. 476, Jan. 2011.
- [32] S. Schwarz, G.-L. Roth, S. Rung, C. Esen, and R. Hellmann, "Fabrication and evaluation of negative axicons for ultrashort pulsed laser applications," *Optics Express*, vol. 28, p. 26207, Aug. 2020.
- [33] "GAEA-2 10 MEGAPIXEL PHASE ONLY LCOS-SLM (REFLECTIVE)." <https://holoeye.com/gaea-4k-phase-only-spatial-light-modulator/>, Oct. 2022.
- [34] Y. Wu, J. Wang, C. Chen, C.-J. Liu, F.-M. Jin, and N. Chen, "Adaptive weighted Gerchberg-Saxton algorithm for generation of phase-only hologram with artifacts suppression," *Optics Express*, vol. 29, p. 1412, Jan. 2021.